Model-Order Reduction of Ion Channel Dynamics Using Approximate Bisimulation

Md. Ariful Islam[a,*], Abhishek Murthy[a,**], Ezio Bartocci[b], Elizabeth M. Cherry[e], Flavio H. Fenton[c], James Glimm[d], Scott A. Smolka[a], Radu Grosu[b]

[a]*Department of Computer Science, Stony Brook University*
[b]*Department of Computer Engineering, Vienna University of Technology*
[c]*School of Physics, Georgia Institute of Technology*
[d]*Department of Applied Mathematics and Statistics, Stony Brook University*
[e]*School of Mathematical Sciences, Rochester Institute of Technology*

Abstract

We show that in the context of the Iyer et al. (IMW) 67-variable cardiac myocyte model, it is possible to replace the detailed 13-state probabilistic model of the sodium channel dynamics with a much simpler Hodgkin-Huxley (HH)-like two-state model, while only incurring a bounded approximation error. We then extend our technique to the 10-state model of the fast recovering calcium-independent potassium channel. The basis of our results is the construction of an approximate bisimulation between the HH-type abstraction and the corresponding detailed ion channel model, both of which are input-controlled (voltage in this case) CTMCs.

The construction of the appropriate approximate bisimulation, as well as the overall result regarding the behavior of this modified IMW model, involves: (1) Identification of the voltage-dependent parameters of the m

*Corresponding author
**Principal corresponding author
Email addresses: mdaislam@cs.stonybrook.edu (Md. Ariful Islam), amurthy@cs.sunysb.edu (Abhishek Murthy)
URL: http://www.eziobartocci.com/ (Ezio Bartocci), http://www.rit.edu/cos/elizabeth-cherry (Elizabeth M. Cherry), https://www.physics.gatech.edu/user/flavio-fenton (Flavio H. Fenton), http://www.ams.sunysb.edu/~glimm/ (James Glimm), http://www.cs.sunysb.edu/~sas/ (Scott A. Smolka), http://ti.tuwien.ac.at/rts/people/grosu/ (Radu Grosu)

and h gates in the HH-type models via a two-step fitting process, carried out over more than 20,000 representative observational traces of the detailed sodium and potassium ion channel models. (2) Proving that the distance between observations of the detailed models and their respective abstraction is bounded. (3) Exploring the sensitivity of the overall IMW model to the HH-type approximations. Our extensive simulation results experimentally validate our findings, for varying IMW-type input stimuli.

Keywords: Model-order reduction, Cardiac cell model, ionic channel, Approximate bisimulation

1. Introduction

The emergence of high throughput data acquisition techniques has changed cell biology from a purely wet lab-based science to also an engineering and information science. The identification of a mathematical model from cellular experimental data, and the use of this model to predict and control the cell's behavior, are nowadays indispensable tools in cell biology's arsenal [22, 4].

Improved data acquisition has led to the creation of increasingly sophisticated partial Differential Equation Models (DEMs) for cardiac cells (myocytes). Their main purpose is to elucidate the biological laws governing the electric behavior of cardiac myocytes, i.e., their underlying ionic processes [5].

Inspired by the squid-neuron DEM [13] developed by Hodgkin-Huxley (HH), Luo and Rudy devised one of the first myocyte DEMs, for guinea pig ventricular cells [19]. Adapting this model to human myocytes led to the ten Tusscher-Noble^2-Panfilov DEM [24], which has 17 state variables and 44 parameters. Based on updated experimental data, Iyer, Mazhari and Winslow (IMW) subsequently developed a DEM comprising of 67 state variables and 94 parameters [15]. This DEM reflects a highly detailed physiological view the electrochemical behavior of human myocytes.

From 17 to 67 variables, all such DEMs capture myocytic behavior at a particular level of abstraction, and hence all of them play an important role in the modeling hierarchy. It is essential, however, to maintain focus on the purpose of a particular DEM; that is, of the particular cellular and ionic processes whose behavior the DEM is intended to capture. Disregarding this purpose may lead to the use of unnecessarily complex DEMs, which may render not only analysis, but also simulation, intractable.

If the only entity of interest is the myocyte's transmembrane voltage, coauthors Cherry and Fenton have experimentally shown that a Minimal Model (MM) consisting of only 4 variables and 27 parameters can accurately capture voltage propagation properties in 1D, 2D, and 3D networks of myocytes [3]. The MM has allowed us to obtain dramatic simulation speedups [1], and to use its linear hybridization as the basis for formal symbolic analysis [12].

Since new technological advances are expected to lead to further insights into myocytic behavior, it is likely that the IMW model will be further refined by adding new variables. As in model checking and controller synthesis, one would therefore like to compute the smallest approximation that is observationally equivalent to the state-of-the-art DEM with respect to the property of interest, modulo some bounded approximation error. This, however, is not easily accomplished, as it implies the automatic approximation of very large nonlinear DEMs.

A first step toward the desired automation is to identify a set of approximation techniques that allow one to systematically remove unobservable variables from say, a detailed model such as IMW to end up with the MM, if the only observable variable is the voltage. This is one of the goals of the project computational modeling and analysis of complex systems [23]. A byproduct of this work is to establish a long-missing formal relation among the existing myocyte DEMs, facilitating the transfer of properties established at one layer of abstraction to the other layers. Building such *towers of abstraction* is becoming increasingly prevalent in systems biology [16, 6].

In this paper we focus on model-order reduction and abstraction of ion channel dynamics. The main question posed in this paper is the following: *Assuming that the conductance of the ion channel is the only observable, is the behavior of an HH-type channel equivalent to the behavior of the IMW channel, modulo a well-defined approximation error?* Specifically, we answer this question for the sodium and the calcium-independent potassium channels. Rather than dealing with behavioral equivalence explicitly, we ask if it is possible to construct an approximate bisimulation [7, 9, 8, 10] between the HH and IMW channel models? This notion of equivalence is stronger than the conventional behavioral equivalence, which compares the observed behaviors (trajectories) of two systems.

The answer to the above-posed question is of broad interest, as it reduces to showing the existence of an approximate bisimulation between two continuous time Markov decision processes; that is, two input-controlled (voltage in this case) Continuous Time Markov Chains (CTMCs). We answer this

question in the positive, by explicitly constructing such a bisimulation. See Fig. 1 for an overview of our approach.

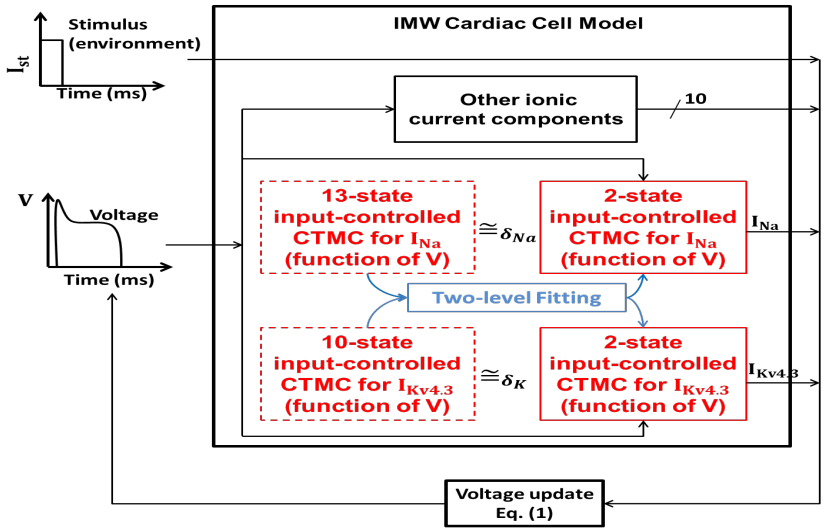

Figure 1: A modular view of the IMW DEM that composes various concurrently evolving components corresponding to the different ionic currents. We replace the 13-state I_{Na} and the 10-state $I_{Kv4.3}$ components with corresponding 2-state HH-type abstractions. A two-level fitting process, described in Section 3, is used to identify the abstractions. Approximate bisimilarity of the detailed components and their corresponding abstractions allows us to substitute them for each other within the whole-cell model. The stimulus current affects the overall voltage update and is not an input to the ionic current components. The system outputs the 13 currents in Eq. (1).

The rest of the paper is organized as follows. Section 2 introduces the the HH and the IMW DEMs and their sodium and potassium channel components. Section 3 presents our parameter identification technique and the resulting HH-type abstraction for the sodium and potassium channels. Section 4 presents empirical evidence of the equivalence of the detailed models and their abstractions. Section 5 proves the existence of an approximate bisimulation between the detailed ion channel models and their abstractions. Section 6 is dedicated to our conclusions and future directions.

2. Background

Cardiac myocytes belong to the class of excitable cells, which also includes neurons. Such cells respond to an external electrical stimulus in the form of an Action Potential (AP), the characteristic change of the transmembrane

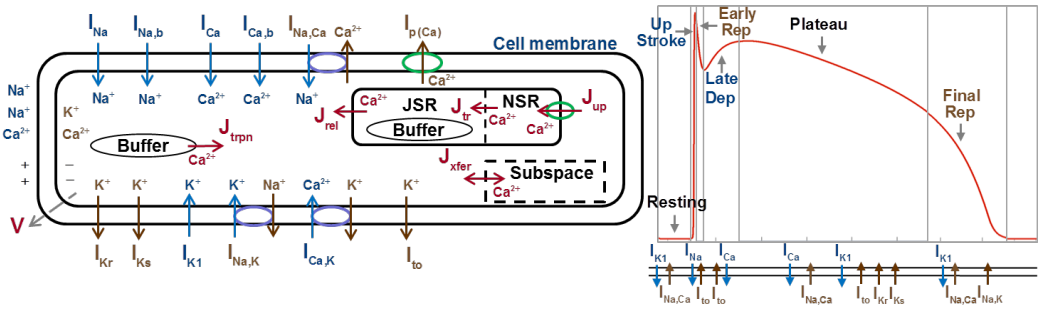

Figure 2: (Left) Currents in IMW: Blue and brown arrows show ionic currents flowing through channels. Blue circles and arrows correspond to ionic exchanger currents and green circles denote ionic pumps. Intracellular currents are shown in Magenta. (Right) The AP, its phases, and associated currents. (Right-Inlay) The sodium current I_{Na} dominates other currents during the upstroke phase. The calcium-independent transient outward Potassium current I_{to1} influences the AP's notch in the early repolarization phase. We focus on one of its two components, the $I_{Kv4.3}$ current.

potential in time as the cell responds to the stimulus. A typical ventricular myocyte AP and its associated phases are shown in Fig. 2(Right). Either an external stimulus, or the diffusing charge from the neighboring cells can excite the myocyte, causing an AP to quickly depolarize the membrane from a negative resting potential of V_{res} mV to a maximum of V_{max} mV followed by gradual repolarization.

2.1. The IMW Cardiac Cell Model

The IMW DEM, a physiologically detailed model, describes the ionic processes responsible for the generation of an AP in human ventricular myocytes:

$$\begin{aligned} -C\dot{V} &= I_{Na}+I_{Nab}+I_{Ca}+I_{Cab}+I_{Kr}+I_{Ks}+I_{K1}+I_{to1}+I_{p(Ca)}+ \\ &\quad I_{NaCa}+I_{NaK}+I_{CaK}+I_{st} \end{aligned} \tag{1}$$

where V is the membrane potential, $\dot{V}$ is its first-order time derivative, C is the membrane's capacitance, and I_v are the ionic currents shown in Fig. 2(Left), except for I_{st}. This is the stimulus current, which could be either an external stimulus or the diffused charge from neighboring cells.

Ionic currents result from the flow of sodium, potassium and calcium ions, across the myocyte's membrane. Three types of transport mechanisms are responsible for these flows: channels, pumps, and exchangers. Ion channels are special proteins that penetrate the membrane's lipid bi-layer, and are selectively permeable to certain ion species. Depending on the conformation of the constituent protein, the channel either allows or inhibits the movement of ions. The protein conformation is voltage dependent, thus the name

voltage-gated channels. All the transmembrane currents in Fig. 2 result from voltage-gated ionic channels, except for I_{NaK}, I_{NaCa}, and $I_{p(Ca)}$, which are exchanger or pump currents.

We focus on the behavior of the sodium channel, which regulates the flow of I_{Na}, a dominant current in the upstroke phase of the AP. The other focus of the paper will be the channel corresponding to the potassium current, $I_{Kv4.3}$. Along with the $I_{Kv1.4}$ current, it constitutes the I_{to1} current, which influences the notch of the AP at the end of early repolarization [11].

2.2. The HH Model for Ion Channels

Hodgkin and Huxley, in their seminal work of [13], model the squid neuron's sodium channel behavior using two independent processes: activation and inactivation. Starting from the resting potential, if the cell is depolarized to a constant voltage, *activation* is responsible for the sudden increase in the channel's conductance. This is followed by *inactivation*, which gradually brings the conductance down, before reaching a steady state. The resulting ionic current is modeled as

$$I_{Na}(V,t) = \overline{g}_{Na}\, m^3(V,t)\, h(V,t)(V - V_{Na}) \tag{2}$$

where $\overline{g}_{Na}$ is the maximum conductance of the sodium channel, and V_{Na} is sodium's Nernst potential. The gating variables $m(V)$ and $(1 - h(V))$ measure the extent of activation and inactivation respectively, with $m = 0$ ($h = 1$) representing complete deactivation (recovery from inactivation) and $m = 1$ ($h = 0$) representing complete activation (inactivation).

The dynamics of m and h are given by the DEM $\mathcal{H}$ as follows.

Definition 1. The DEM $\mathcal{H}$ gives the **dynamics of** m **and** h, both $\in \mathbb{R}_{\geq 0}$:

$$\dot{m} = \alpha_m(V)(1 - m) - \beta_m(V)m, \qquad \dot{h} = \alpha_h(V)(1 - h) - \beta_h(V)h$$

The linear system obtained by fixing $V = v$ will be denoted as $\mathcal{H}^v$. The conductance of a channel modeled using by m and h is given by:

$$O_H(V,t) = m(V,t)^\lambda h(V,t) \tag{3}$$

where λ is the degree of activation[1], and is 3 in [13]. The rate functions $\alpha_x(V)$ and $\beta_x(V), x \in \{m, h\}$ are continuous in V, and for the sodium channel are given by Eqs. (20)-(21) and Eqs. (23)-(24) of [13].

[1]In this paper, we consider the degree of inactivation to be 1 for reducing the sodium and potassium channels.

In the Voltage Clamp Experiments (VCEs) performed by the authors in [13], the membrane potential was initially maintained at the resting potential V_{res}. In each of the VCE, the membrane potential was suddenly changed to a clamp potential V_c and the emanating ionic current and conductance was observed till steady state. The dynamics of the gating variables m and h, during a VCE is given by:

$$x(V = V_c, t) = x_\infty - (x_\infty - x_0)exp(-t/\tau_x), \quad x \in \{m, h\} \tag{4}$$

where the parameters $x_\infty(V_c) = \alpha_x(V_c)/(\alpha_x(V_c) + \beta_x(V_c))$, $\tau_x = 1/(\alpha_x(V_c) + \beta_x(V_c))$ and $x_0(V_c) = x_\infty(V_{res})$, $x \in \{m, h\}$. Eq. (3) was then fit to the observed current to estimate the parameters.

2.3. Voltage-Controlled CTMC Models

The IMW model uses physiologically detailed models to capture the behavior of ion channels. The voltage-dependent conformations of the constituent protein are captured as states of a stochastic model. Continuous functions of voltage are employed for transfer rates between the states.

In the IMW model, the sodium current, I_{Na}, is modeled by an equation similar to Eq. (2). The conductance of the HH-type channel, m^3h, is replaced by $O_{Na}(V, t) = O_1(V, t) + O_2(V, t)$, the sum of the occupancy probabilities of the two states of the stochastic model shown in Fig. 3 [18, 14] and defined as follows.

Definition 2. Consider the 13-state model for sodium-channel dynamics shown in Fig. 3. Let p_j denote the j^{th} state occupancy probability from the vector $\mathbf{p} = [C_0, C_1, C_2, C_3, C_4, O_1, O_2, C_0I, C_1I, C_2I, C_3I, C_4I, I]^T \in \mathbb{R}^{13}_{\geq 0}$. The **evolution of p** is described by the model $\mathcal{M}_{Na}$ as:

$$\dot{p}_j = \sum_{i \neq j} k_{ij}(V)p_i - \sum_{i \neq j} k_{ji}(V)p_j \qquad i, j = 1, \ldots, 13 \tag{5}$$

where $\dot{p}_j$ denotes the time derivative of p_j, V is the transmembrane potential, and $k_{ij}(V) \in \mathbb{R}_{\geq 0}$ is the transition rate from the i^{th} to the j^{th} state as defined in Table 1. This system can be re-written as:

$$\dot{\mathbf{p}} = A^{Na}(V).\mathbf{p}, \tag{6}$$

where $A^{Na}(V)$ is a 13×13 matrix with $A^{Na}_{j,i}(V) = k_{ij}(V)$ $i \neq j$, $A^{Na}_{j,j}(V) = -\sum_{i \neq j} k_{ji}$. The linear system $\mathcal{M}^v_{Na}$ is obtained by fixing $V = v$ in Eq. 6. The conductance (output) of the model is given by $O_1 + O_2$.

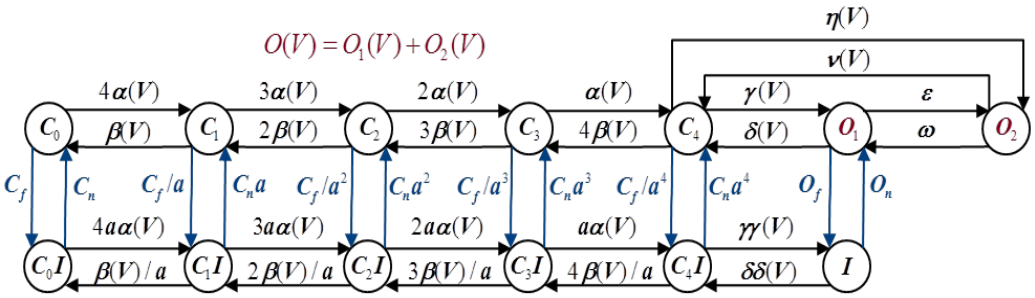

Figure 3: The 13-variable voltage-controlled CTMC, $\mathcal{M}_{Na}$, for the sodium channel component of the IMW model. The conductance of the channel is the sum of occupancy probabilities $O = O_1 + O_2$. The transition rates are defined in Table 1.

rate	function	rate	function	rate	function
$\alpha(V)$	$c.e^{-19.6759+0.0113V}$	$\delta\delta(V)$	$c.e^{-38.4839-0.1440V}$	ϵ	0.0227
$\beta(V)$	$c.e^{-26.2321-0.0901V}$	$\gamma\gamma(V)$	$c.e^{-21.9493+0.0301V}$	ω	1.0890
$\gamma(V)$	$c.e^{-16.5359+0.1097V}$	$\eta(V)$	$c.e^{-19.6729+0.0843V}$	c_n	0.7470
$\delta(V)$	$c.e^{-27.0926-0.0615V}$	$O_n(V)$	$c.e^{-20.6726+0.0114V}$	c_f	0.2261
$\nu(V)$	$c.e^{-26.3585-0.0678V}$	$O_f(V)$	$c.e^{-39.7449+0.0027V}$	a	1.4004

Table 1: Transfer rates of $\mathcal{M}_{Na}$, which is shown in Fig. 3. Values were instantiated from Table 6 of [15] at temperature T = 310K, and $c = 8.513 \times 10^9$.

The potassium current $I_{Kv4.3}$ in the IMW DEM is modeled by

$$I_{Kv4.3} = \overline{g}_{Kv4.3}\,(O_K(V))\,(V - V_K) \tag{7}$$

where $\overline{g}_K$ is the maximum conductance of the channel, V_K is the Nernst potential for potassium, $O_K(V) = O(V)$ is the occupancy probability of the open state in the 10-state voltage-controlled CTMC shown in Fig. 4 [11] and defined as follows.

Definition 3. Consider the 10-state model for the potassium channel component shown in Fig. 4. Let q_j denote the j^{th} state occupancy probability from the vector $\mathbf{q} = [C_0, C_1, C_2, C_3, O, CI_0, CI_1, CI_2, CI_3, OI]^T \in \mathbb{R}^{10}_{\geq 0}$. The **evolution of q**, as described by the model $\mathcal{M}_K$, is given by

$$\dot{q}_j = \sum_{i \neq j} k_{ij}(V) q_i - \sum_{i \neq j} k_{ji}(V) q_j \qquad i, j = 1, \ldots, 10 \tag{8}$$

where $\dot{q}_j$ denotes the time derivative of q_j, V is the transmembrane potential, and $k_{ij}(V) \in \mathbb{R}_{\geq 0}$ is the transition rate from the i^{th} to the j^{th} state as defined

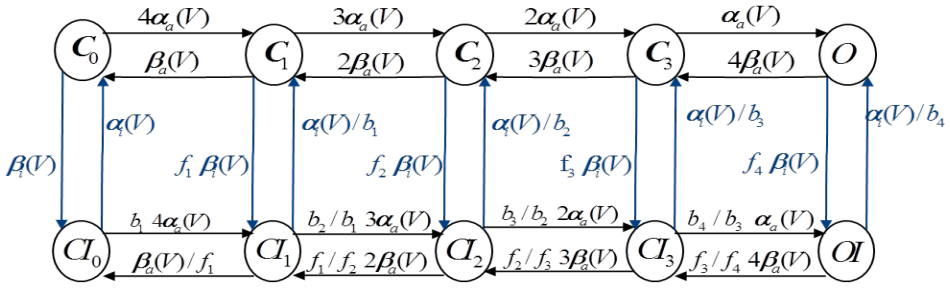

Figure 4: The 10-variable voltage-controlled CTMC, $\mathcal{M}_K$, for the potassium channel component of the IMW model. The conductance of the channel is the occupancy probability O. The transition rates are defined in Table 2.

in Table 2. This system can be re-written as:

$$\dot{\mathbf{q}} = A^K(V).\mathbf{q}, \tag{9}$$

where $A^K(V)$ is a 10×10 matrix with $A^K_{j,i}(V) = k_{ij}(V)$ $i \neq j$, $A^K_{j,j}(V) = -\sum_{i \neq j} k_{ji}$. The linear system $\mathcal{M}^v_K$ is obtained by fixing $V = v$ in Eq. 9. The conductance (output) of the model is given by O.

rate	function	rate	function	rate	function
$\alpha_a(V)$	$0.5437e^{0.029V}$	f_1	1.8936	b_1	6.7735
$\beta_a(V)$	$0.0802e^{0.0468V}$	f_2	14.2246	b_2	15.6213
$\alpha_i(V)$	$0.0498e^{0.0004V}$	f_3	158.5744	b_3	28.7533
$\beta_i(V)$	$0.0008e^{(5.374\times10^{-8}V)}$	f_4	142.9366	b_4	524.5762

Table 2: Transfer rates of $\mathcal{M}_K$, shown in Fig. 4. $c = 8.513\times10^9$. Note that these values are different from the ones given in Table 9 of [15]. Corrections were made to the parameters to match the observed APs of the IMW model.

3. Model-Order Reduction of Ion Channel Dynamics

We construct two HH-type DEMs, $\mathcal{H}_{Na}$ and $\mathcal{H}_K$, that can be substituted for the components $\mathcal{M}_{Na}$ and $\mathcal{M}_K$ respectively within the IMW cardiac-cell model. We perform the following abstractions in the process:

- The abstractions $\mathcal{H}_{Na}$ and $\mathcal{H}_K$ employ three and four activating subunits respectively. A single subunit is used to model inactivation.

- We abstract away the conditional dependence between activation and inactivation. This is done by abstracting away the scaling factors: a of $\mathcal{M}_{Na}$ and $f_1 - f_4$, $b_1 - b_4$ of $\mathcal{M}_K$.

After identifying $\mathcal{H}_{Na}$, its conductance, m^3h, is substituted for $\mathcal{M}_{Na}$'s conductance, $O_1 + O_2$, in the IMW model's version of Eq. (2). Similarly $\mathcal{H}_K$'s conductance, m^4h, replaces $\mathcal{M}_K$'s conductance, O_K in Eq. (7). Note that this leads to two levels of substitution. First, the conductance of the detailed ionic current components is substituted by the abstract model conductances. Then the modified current component replaces the original term in Eq. (1).

Our approach to obtaining the 2-state HH-type abstractions $\mathcal{H}_{Na}$ and $\mathcal{H}_K$ from the detailed models, $\mathcal{M}_{Na}$ and $\mathcal{M}_K$ respectively, is summarized in Fig. 5, and described as follows.

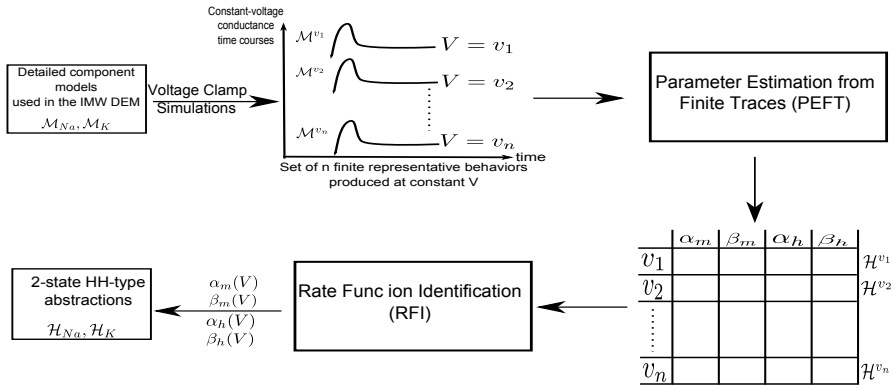

Figure 5: Abstraction process for ion channel dynamics. The voltage-controlled CTMC components are simulated at constant voltages (clamp potentials) using the steady state values corresponding to $V = V_{res}$ as the initial conditions. The conductance time courses are then fit as per Eq. (3) to obtain the parameters $\alpha_m, \beta_m, \alpha_h, \beta_h$ at the clamp potentials used for voltage clamp simulations. The four parameter values, along with the initial conditions determine the $\mathcal{H}^v$ abstractions. The parameters are then fit in the RFI step to obtain parameter functions $\alpha_m(V), \beta_m(V), \alpha_h(V), \beta_h(V)$.

1. **Voltage clamp simulations**
   VCEs, pioneered by Hodgkin and Huxley in their seminal work of [13], are intended to expose the activation and inactivation processes governing a channel's behavior. The experiments involve stimulating the channel by changing the membrane potential suddenly and then holding it constant, starting from appropriate initial conditions. As the ion channel reacts by opening, and then closing, the resulting ionic currents

are recorded. The corresponding conductance time courses characterize the channel's response to varying the membrane potential.

We simulated VCEs by simulating the detailed models, $\mathcal{M}_{Na}$ and $\mathcal{M}_K$, for various values of V. In other words, the systems of linear differential equations, $\mathcal{M}^v_{Na}$ and $\mathcal{M}^v_K$, were simulated for different values of $V_{res} \leq v \leq V_{max}$. We used 20,000 uniformly spaced voltage values for v, and the corresponding $\mathcal{M}^v_{Na}$ and $\mathcal{M}^v_K$ were simulated using MATLAB's ODE45 solver [20], starting from the initial conditions specified in Table 4 of [15]. The initial conditions correspond to the steady state of the models at $v = V_{res}$. This is exactly the initially conditions used by Hodgkin and Huxley in [13]. The resulting conductance time courses, $O_1(t) + O_2(t)$ for $\mathcal{M}^v_{Na}$ and $O(t)$ for $\mathcal{M}^v_K$, were recorded until steady state was reached. As per Theorem 3 in Appendix A, for all $v \in [V_{res}, V_{max}]$, $\mathcal{M}^v_{Na}$ and $\mathcal{M}^v_K$ have stable equilibria and therefore steady state is guaranteed. Simulating the models at constant voltage values corresponds to the clamp potentials to which the membrane was excited in [13] to uncover the activation and inactivation process.

2. **Parameter Estimation from Finite Traces (PEFT)**
PEFT is a procedure that identifies $\mathcal{H}^v_{Na}$ and $\mathcal{H}^v_K$ models corresponding to $\mathcal{M}^v_{Na}$ and $\mathcal{M}^v_K$ respectively. The parameters $\alpha^v_m, \beta^v_m, \alpha^v_h, \beta^v_h$ are estimated such that the resulting conductance time courses, produced by $\mathcal{H}^v_{Na}$ and $\mathcal{H}^v_K$, match the conductance time courses observed in the voltage clamp simulations for $\mathcal{M}^v_{Na}$ and $\mathcal{M}^v_K$ respectively.

   In our implementation, we fit $\mathcal{M}^v_{Na}$'s conductance time series, $O_1(t) + O_2(t)$, to $\mathcal{H}^v_{Na}$'s $m^3(t)h(t)$. Time series $O(t)$ observed from $\mathcal{M}^v_K$ was fit with $m^4(t)h(t)$ to identify $\mathcal{H}^v_{Na}$. At constant voltage v, the trajectories $m(t)$ and $h(t)$ of $\mathcal{H}^v_{Na}$ and $\mathcal{H}^v_K$ are given by

$$z(t) = \frac{\alpha^v_z}{\alpha^v_z + \beta^v_z} + \left(z(0) - \frac{\alpha^v_z}{\alpha^v_z + \beta^v_z} \right) \exp\left(- \left(\alpha^v_z + \beta^v_z \right) t \right) \tag{10}$$

   where $z \in \{m, h\}$ and $x \in \{Na, K\}$. The fitting was performed using MATLAB's curve fitting utility *cftool* [21] for each voltage value v used in the voltage clamp simulations. Two aspects of our implementation deserve further elaboration:

   - **Choosing $m(0)$ and $h(0)$** - The initial conditions were chosen such that for $\mathcal{H}^v_{Na}$, $m(0)^3h(0)$ and for $\mathcal{H}^v_K$, $m(0)^4h(0)$ was approximately equal to $O_{V_{res}}$, the steady state conductances of $\mathcal{M}^{V_{res}}_{Na}$

and $\mathcal{M}_K^{V_{res}}$ respectively. As per convention, we also ensured that $m^v(0) \approx 0$ and $h(0) \approx 1$ for both the models. We chose $m(0) = 0.0027, h(0) = 0.95$ for $\mathcal{H}_{Na}^v$; $m(0) = 0.00138, h(0) = 0.98$ for $\mathcal{H}_{Na}^v$.

- **Providing seed-values** - For each voltage-value v, *cftool* needs seed values of α_x^v, β_x^v, $x \in \{m, h\}$, to start optimizing over the parameter space. The parameters estimated for the i^{th} voltage v_i were used as seed-values for v_{i+1}. For $i = 0$, when $v = v_{res}$, the parameters were calculated by trial and error.

3. **Rate Function Identification (RFI)**
RFI is a procedure that fits the parameter values, α_m^v, β_m^v, α_h^v and β_h^v, as functions of voltage to produce the parameter functions $\alpha_m(V)$, $\beta_m(V)$, $\alpha_h(V)$ and $\beta_h(V)$. We fit exponential functions using *cftool* [21]. The parameter functions defining $\mathcal{H}_{Na}$ and $\mathcal{H}_K$ are as follows.

Rate functions that define $\mathcal{H}_{Na}$:

$$\alpha_m(V) = \begin{cases} 13.63 - \frac{14.3}{1+\exp(0.061V+1.72)} & V \leq 19.98 \\ 20.76 - \frac{7.89}{1+\exp(464.1V-13920)} & V > 19.98 \end{cases}$$

$$\beta_m(V) = \begin{cases} 9.925 & V \leq -65 \\ 4.7 - \frac{2.58}{1+\exp(0.61V+38.19)} & -65 < V \leq 5.8 \\ 12.24 - \frac{7.77}{1+\exp(1877V-56314)} & V > 5.8 \end{cases}$$

$$\alpha_h(V) = \frac{0.1745}{1 + \exp(269.8V + 17720)}$$

$$\beta_h(V) = 10.1 - \frac{10}{1 + \exp(0.0579V + 0.71)}$$

Rate functions that define $\mathcal{H}_K$

$$\alpha_m(V) = \begin{cases} 0.45\exp(0.026V) & V \leq 24.5 \\ 0.85 - \frac{0.048}{1+\exp(-0.2V+9.5)} & V > 24.5 \end{cases}$$

$$\beta_m(V) = \begin{cases} 0.029\exp(0.065V) & V \leq 24.5 \\ 0.1839 - \frac{0.05}{1+\exp(0.19V-9.32)} & V > 24.5 \end{cases}$$

$$\alpha_h(V) = 0.0015 - \frac{0.0014}{1 + \exp(0.027V - 2.54)}$$

$$\beta_h(V) = \begin{cases} 0.12 - \frac{0.06}{1+\exp(-0.054V+2.62)} & V \leq 24.5 \\ 0.109 + \frac{0.015}{1+\exp(-0.033V+10.83)} & V > 24.5 \end{cases}$$

Adapting the Abstraction Process to Arbitrary Observable Functions of $\mathcal{M}_{Na}$ and $\mathcal{M}_{\mathcal{K}}$: The two-step abstraction process, consisting of PEFT and RFI, assumed that the conductance of the detailed models was the observable function for them. In other words, $O_1(V,t) + O_2(V,t)$ for $\mathcal{M}_{Na}$, and $O(V,t)$ for $\mathcal{M}_K$ mapped a state of the corresponding model to its output. The abstraction methodology described above is not restricted by these observable functions and can be adapted to arbitrary functions that map a state to its output.

Suppose we are given a stochastic (detailed) ion channel model $\mathcal{M}$, with a function that maps the state occupancy probability vector to a real-valued output. The goal is to reduce it to an HH-type abstraction, $\mathcal{H}$, that has a degree of activation λ and 1 as the degree of inactivation. We provide details for modifying PEFT, such that the resulting set of constant-voltage $\mathcal{H}^v$ systems are behaviorally equivalent to constant-voltage versions, $\mathcal{M}^v$, of the detailed model.

The first step is to establish a mapping between the states of $\mathcal{M}$ and a $2(\lambda+1)$-state stochastic model corresponding to the HH-type model, denoted by $\mathcal{H}_{stoch}$. We will label the states of $\mathcal{H}_{stoch}$ as x_{ij}, and denote the corresponding occupancy probability by p_{ij} where $i = 0, \ldots, \lambda$ and $j = 0, 1$. The model $\mathcal{H}_{stoch}$ interprets the degrees of activation and inactivation as the number of independent activating and inactivating subunits of the channel. In our case, the state x_{ij} corresponds to the conformation of the channel where i activating and j inactivating subunits are in an "open" state that allow ion flow. Fig. 6 shows the model $\mathcal{H}_{stoch}$ corresponding to an HH-type model with $\lambda = 3$ and a degree of inactivation of 1. In the model, the state x_{21} corresponds to the a conformation where the inactivating subunit and two of the activating subunits are open. The inactivating subunit can close at a rate of $\beta_h(V)$ and change the conformation to x_{20}. The remaining activating subunit can open at the rate of $\alpha_m(V)$ to change the state to x_{31}. In this conformation, all the three activating subunits and the inactivating subunit are open. Thus, this state corresponds to the conformation of the channel which allows ion flow. From the state x_{21}, any of the two independent activating subunits could close at a rate of $2\beta_m(V)$ to change the state to x_{11}. Once we have mapped the states of the given stochastic model to the states of $\mathcal{H}_{stoch}$, PEFT can be modified to identify $\mathcal{H}^v_{stoch}$ systems that can match the behavioral traces observed from $\mathcal{M}^v$.

The two-state HH-type model forms an invariant manifold [17] of $\mathcal{H}_{stoch}$. The occupancy probability of the state x_{ij} is given by $m^i h^j$. This correspon-

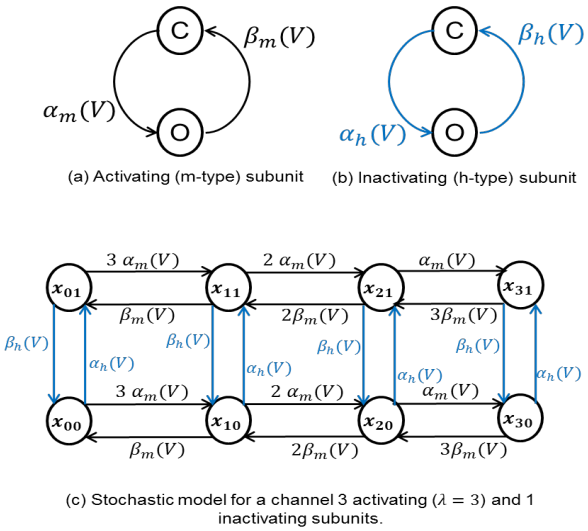

Figure 6: Invariant manifolds can be used to map the states of a $2(\lambda+1)$-state stochastic model to an HH-type model with a degree of activation λ and degree of inactivation 1 ($\lambda = 3$ in the example).

dence helps us map a state vector of $\mathcal{H}_{stoch}$ to a state of the HH-type model (the vector $[m, h]^T$). Note that this mapping is exact and provides an output function that can be matched to the output function of $\mathcal{M}$. Suppose the output function maps states of $\mathcal{M}$ corresponding to the states x_{11} and x_{31} under the established mapping. Then the output function of $\mathcal{H}$ will take as arguments mh and m^3h. PEFT can be used to minimize divergence of this new observation function to identify $\mathcal{H}^v$ systems.

4. Results

The component models, $\mathcal{M}_{Na}$ and $\mathcal{M}_K$, were substituted by their respective HH-type abstractions $\mathcal{H}_{Na}$ and $\mathcal{H}_K$ within the whole-cell IMW model. The substitutions were done in three combinations: 1) substitution of $\mathcal{M}_{Na}$ only, 2) substitution of $\mathcal{M}_K$ only, and 3) substitution of both $\mathcal{M}_{Na}$ and $\mathcal{M}_K$. The modified IMW models were simulated in FORTRAN in all three cases with an integration time step of 0.001 ms. Both supra- and sub-threshold stimuli, lasting 0.5 ms, were used to excite the cardiac cell. Supra-threshold stimuli used were: $S1 = -100$ pA/pF, and $S2 = -120$ pA/pF. Sub-threshold stimuli employed were: $S3 = -10$ pA/pF, and $S4 = -20$ pA/pF.

Fig. 7 provides empirical evidence of the modified whole cell models being behaviorally equivalent to the original models. The model retains both

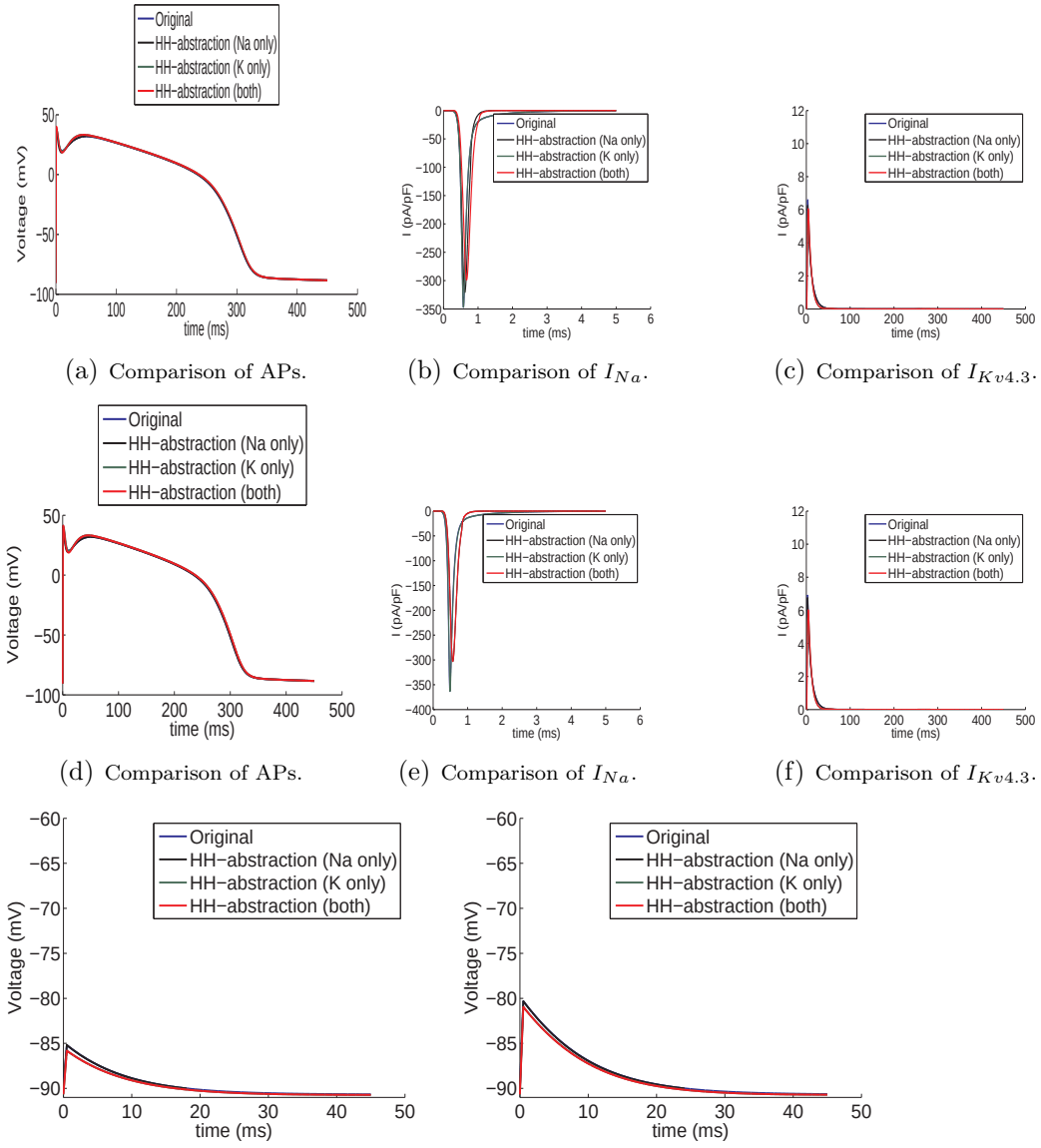

(a) Comparison of APs. (b) Comparison of I_{Na}. (c) Comparison of $I_{Kv4.3}$.

(d) Comparison of APs. (e) Comparison of I_{Na}. (f) Comparison of $I_{Kv4.3}$.

(g) Comparison of APs ($S3$). (h) Comparison of APs ($S4$).

Figure 7: Comparison of the original and the modified IMW models when $\mathcal{M}_{Na}$ and $\mathcal{M}_K$ are substituted by $\mathcal{H}_{Na}$ and $\mathcal{H}_K$ respectively. Subfigures (a)-(c) are obtained for the S1 stimulus, (d)-(f) for the S2 stimulus, (g) for the S3 stimulus and (h) for the S4 stimulus. S1 and S2 are supra-threshold stimuli and lead to an AP, whereas S3 and S4 being subthreshold stimuli fail to produce the AP.

S	V (mV)			I_{Na} (pA/pF)			I_K (pA/pF)		
	Na Only	K Only	Both	Na Only	K Only	Both	Na Only	K only	Both
S1	7.73×10^{-4}	1.4×10^{-3}	1.6×10^{-3}	2.7×10^{-3}	8.3×10^{-6}	5.2×10^{-3}	6.2×10^{-5}	1.72×10^{-4}	1.1×10^{-3}
S2	7.3×10^{-4}	1.4×10^{-3}	1.5×10^{-3}	5.2×10^{-3}	5.4×10^{-5}	5.2×10^{-2}	4.67×10^{-5}	2.54×10^{-4}	2.5×10^{-4}
S3	1.61×10^{-5}	1.1×10^{-3}	1.1×10^{-3}	-	-	-	-	-	-
S4	1.39×10^{-4}	1.2×10^{-3}	1.3×10^{-3}	-	-	-	-	-	-

Table 3: Mean L2 errors incurred in the simulations after substituting $\mathcal{M}_{Na}$ by $\mathcal{H}_{Na}$ and $\mathcal{M}_K$ by $\mathcal{H}_K$ in the IMW model. The first column, S, stands for the stimulus used to excite the cell at the beginning of the simulation. Only the voltage errors were recorded for the sub-threshold stimuli S3 and S4 as the currents were negligible.

normal and anomalous cell-level behaviors on replacing the 13-state sodium channel and/or 10-state potassium channel components with the corresponding 2-state abstraction(s). In the next section, we formalize the equivalence of $\mathcal{M}_{Na}$ and $\mathcal{M}_K$ to $\mathcal{H}_{Na}$ and $\mathcal{H}_K$ respectively using approximate bisimulation.

5. Approximate Bisimulation Equivalence of M_I and M_H

In this section, we formalize the equivalence of the the detailed ion channel models, $\mathcal{M}_{Na}$ and $\mathcal{M}_K$, and their HH-type abstractions, $\mathcal{H}_{Na}$ and $\mathcal{H}_K$. Proposed in [10], the concept of *approximate bisimulation* enables us to formalize the approximate equivalence of two dynamical systems. The conventional notion of behavioral equivalence compares the trajectories of the two systems. Approximate bisimulation is stronger than approximate behavioral equivalence in that it allows for compositional reasoning. We will use the following two dynamical systems to define approximate bisimulation in a way similar to [9]:

$$\Delta_i : \begin{cases} \dot{\mathbf{x}}_i(t) & = f_i(\mathbf{x}_i(t), \mathbf{u}_i(t)) \\ \mathbf{y}_i(t) & = g_i(\mathbf{x}_i(t)) \end{cases}, i = 1, 2. \tag{11}$$

with the state vectors $\mathbf{x}_i \in \mathbb{R}^{n_i}$, the input vectors $\mathbf{u}_i \in \mathbb{R}^m$ and the output vectors $\mathbf{y}_i \in \mathbb{R}^p$. We assume that the dynamics are given by Lipschitz-

continuous functions $f_i : \mathbb{R}^{n_i} \times \mathbb{R}^{n_i} \to \mathbb{R}^{n_i}$, $i = 1, 2$. We use $\mathbf{X}_i^0 \subseteq \mathbb{R}^{n_i}, i = 1, 2$, to denote the set of initial conditions for the two dynamical systems.

In our case, the ion channel models $\mathcal{M}_{Na}$ and $\mathcal{M}_K$ are dynamical systems with 13 and 10-dimensional state vectors, $\mathbf{p} \in \mathbb{R}^{13}_{\geq 0}$ and $\mathbf{q} \in \mathbb{R}^{10}_{\geq 0}$, respectively. The dynamics of $\mathbf{p}$ and $\mathbf{q}$, corresponding to $f(.,.)$ in Eq. (11), are given by Eqs. (6) and (9) respectively. Both models receive voltage, a 1-dimensional input and produce conductance, a 1-dimensional output. The output functions are $g_{Na}(\mathbf{p}) = O_1 + O_2$ and $g_{Na}(\mathbf{q}) = O$ as per Definitions 2 and 3. Table 4 of [15] provides the initial conditions for the two models. Both models have a single initial condition.

The HH-type abstractions, $\mathcal{H}_{Na}$ and $\mathcal{H}_K$, on the other hand have 2-dimensional state vectors, $[m_{Na}, h_{Na}]^T$ and $[m_K, h_K]^T$ respectively. The dynamics are as per Definition 1. The rate functions defining the two models were identified in the RFI step and are given in Section 3. Voltage, the input, and conductance, the output, are both 1-dimensional. The output function, as per Definition 1 is $m_i^\lambda h_i$, $i \in \{Na, K\}$, where $\lambda = 3$ for $\mathcal{H}_{Na}$ and $\lambda = 4$ for $\mathcal{H}_K$. In Section 3, PEFT identified the singleton initial conditions for them.

Definition 4. The two dynamical systems defined in Eq. (11) are said to be *approximately bisimilar with precision* δ, denoted by $\Delta_1 \cong_\delta \Delta_2$, if there exists a relation $B_\delta \subseteq \mathbb{R}^{n_1} \times \mathbb{R}^{n_2}$ such that:

1. For every $\mathbf{x}_1 \in \mathbf{X}_1^0$, there exists $\mathbf{x}_2 \in \mathbf{X}_2^0$ such that $(\mathbf{x}_1, \mathbf{x}_2) \in B_\delta$.
2. For every $(\mathbf{x}_1, \mathbf{x}_2) \in B_\delta$, $d(\mathbf{y}_1, \mathbf{y}_2) \leq \delta$, where $\mathbf{y}_1$ and $\mathbf{y}_2$ are the corresponding outputs and d is a metric distance defined on $\mathbb{R}^p$.
3. For every $(\mathbf{x}_1, \mathbf{x}_2) \in B_\delta$, for all $T > 0$,
   (a) If on the input signal $\mathbf{u}(t)$, Δ_1 produces the trajectory $\mathbf{x}_1(t)$, where $\mathbf{x}_1(0) = \mathbf{x}_1$, then Δ_2 evolves as per the trajectory $\mathbf{x}_2(t)$, where $\mathbf{x}_2(0) = \mathbf{x}_2$, such that $(\mathbf{x}_1(t), \mathbf{x}_2(t)) \in B_\delta$ for all $t \in [0, T]$.
   (b) If on the input signal $\mathbf{u}(t)$, Δ_2 produces the trajectory $\mathbf{x}_2(t)$, where $\mathbf{x}_2(0) = \mathbf{x}_2$, then Δ_1 evolves as per the trajectory $\mathbf{x}_1(t)$, where $\mathbf{x}_1(0) = \mathbf{x}_1$, such that $(\mathbf{x}_1(t), \mathbf{x}_2(t)) \in B_\delta$ for all $t \in [0, T]$.

It should be noted that Definition 4 also applies when Δ_1 and Δ_2 are autonomous systems, i.e. they do not evolve according to an explicit input signal. In that case, the input signal can be considered as time. B_δ, which is

used to denote the approximate bisimulation relation, contains corresponding states from trajectories of the two systems. These trajectories must be initialized from states related by B_δ. The constant voltage versions of the ion channel models, $\mathcal{M}^v_{Na}$ and $\mathcal{M}^v_K$, and their corresponding HH-type abstractions, $\mathcal{H}^v_{Na}$ and $\mathcal{H}^v_K$, are examples of autonomous dynamical systems. For all voltage values, the initial conditions of $\mathcal{M}^v_{Na}$ and $\mathcal{M}^v_K$ are the same as that of $\mathcal{M}_{Na}$ and $\mathcal{M}^K$ respectively. Similarly, for all voltage values, the initial conditions of $\mathcal{H}^v_{Na}$ and $\mathcal{H}^v_K$ are the same as that of $\mathcal{H}_{Na}$ and $\mathcal{H}_K$ respectively. Next, we state a lemma that leads to the approximate bisimilarity of the constant-voltage abstractions, $\mathcal{H}^v_{Na}$ and $\mathcal{H}^v_K$, and their corresponding detailed models $\mathcal{M}^v_{Na}$ and $\mathcal{M}^v_K$.

Lemma 1. *Consider the voltage values $v \in [V_{res}, V_{max}]$ that were used to simulate and fit the trajectories of, $\mathcal{M}^v_{Na}$ and $\mathcal{M}^v_K$ in PEFT. The corresponding HH-type abstractions $\mathcal{H}^v_{Na}$ and $\mathcal{H}^v_K$ are approximately bisimilar to the detailed models, i.e. $\mathcal{M}^v_{Na} \cong_{\delta^v_{Na}} \mathcal{H}^v_{Na}$ and $\mathcal{M}^v_K \cong_{\delta^v_K} \mathcal{H}^v_K$. The errors δ^v_{Na} and δ^v_K are the maximum errors incurred by the PEFT procedure while fitting the trajectories of $\mathcal{M}^v_{Na}$ and $\mathcal{M}^v_K$ respectively.*

Proof. Theorem 3 in Appendix A proves that for all the voltage values $v \in [V_{res}, V_{max}]$, the corresponding $\mathcal{M}^v_{Na}$ and $\mathcal{M}^v_K$ have stable equilibria. The fitting performed by PEFT ensures that the corresponding HH-type abstractions $\mathcal{H}^v_{Na}$ and $\mathcal{H}^v_K$ also reach their steady state.

Let δ^v_{Na} and δ^v_K be the maximum error incurred by cftool while fitting the trajectories of $\mathcal{M}^v_{Na}$ and $\mathcal{M}^v_K$, respectively. The approximate bisimulation relation $B_{\delta^v_{Na}}$ relates the corresponding states on the unique trajectories of the two systems. Two states on the two trajectories are related if they are reached from their respectively initial conditions in the same time.

We are guaranteed that the errors in the observations will not deviate more than δ^v_{Na} and δ^v_K as the respective pairs of systems reach their steady state, thus ensuring $\mathcal{M}^v_{Na} \cong_{\delta^v_{Na}} \mathcal{H}^v_{Na}$ and $\mathcal{M}^v_K \cong_{\delta^v_K} \mathcal{H}^v_K$. □

Theorem 2. *Let $\mathcal{V}$ be the set of input signals, denoted by $V(t)$, such that $V(0) = V_{res}$ and the signals reach the resting potential, V_{res}, infinitely often. If the type of input signals are restricted to $\mathcal{V}$, then $\mathcal{M}_{Na} \cong_{\delta_{Na}} \mathcal{H}_{Na}$ and $\mathcal{M}_K \cong_{\delta_K} \mathcal{H}_K$, where $\delta_{Na} = 6 \times 10^{-3}$ and $\delta_K = 0.15$.*

Proof. Consider the input signal $V(t) \in \mathcal{V}$. As this input signal is provided to $\mathcal{M}_{Na}$ and $\mathcal{H}_{Na}$, we will compare the resulting trajectories $\mathbf{p}(t)$ and

$[m_{Na}(t), h_{Na}(t)]^T$. A similar treatment will be given to the trajectories, $\mathbf{q}(t)$ and $[m_K(t), h_K(t)]^T$, of $\mathcal{M}_K$ and $\mathcal{H}_K$ respectively.

Consider the time interval $[t, t+\delta t]$. In the limit $\delta t \to 0$, we can consider the input $V(t) = v$ for $t \in [t, t+\delta t]$. The evolution of $\mathcal{M}_{Na}$ and $\mathcal{H}_{Na}$ in the interval $[t, t+\delta t]$ can be approximated by the evolution of the constant voltage dynamical systems $\mathcal{M}^v_{Na}$ and $\mathcal{H}^v_{Na}$ respectively.

For every voltage value v that the input signal $V(t)$ can take over the interval $[t, t+\delta t]$, there will be a value $v^* \in [V_{res}, V_{max}]$, which is closest to it among the voltage values used to simulate $\mathcal{M}^{v^*}_{Na}$ during PEFT. Thus, the divergence between the trajectories of $\mathcal{M}^v_{Na}$ and $\mathcal{H}^v_{Na}$ in the interval $[t, t+\delta t]$ can be broken down into three components:

- Divergence between $\mathcal{M}^v_{Na}$ and $\mathcal{M}^{v^*}_{Na}$
- Divergence between $\mathcal{M}^{v*}_{Na}$ and $\mathcal{H}^{v^*}_{Na}$
- Divergence between $\mathcal{H}^{v*}_{Na}$ and $\mathcal{H}^v_{Na}$

As per Lemma 1, $\mathcal{M}^{v^*}_{Na} \cong_{\delta^{v^*}_{Na}} \mathcal{H}^{v^*}_{Na}$. This ensures that the divergence between $\mathcal{M}^{v^*}_{Na}$ and $\mathcal{H}^{v^*}_{Na}$ is bounded by $\delta^{v^*}_{Na}$.

The divergence between $[m^{v^*}_{Na}(t), h^{v^*}_{Na}(t)]^T$, the trajectory of $\mathcal{H}^{v*}_{Na}$, and $[m^v_{Na}(t), h^v_{Na}(t)]^T$, the trajectory of $\mathcal{H}^v_{Na}$, can be bound using sensitivity analysis. We bound the sensitivity of the solutions $m_{Na}(t)$ and $h_{Na}(t)$ to a change in voltage from v to v^*. The sensitivity is bounded by taking the partial derivative of the solution in Eq. (4) with respect to the voltage V. Using chain rule we have,

$$\frac{\partial m}{\partial V} = \frac{\partial m}{\partial m_\infty}.\frac{\partial m_\infty}{\partial V} + \frac{\partial m}{\partial \tau_m}.\frac{\partial \tau_m}{\partial V} \qquad \frac{\partial h}{\partial V} = \frac{\partial h}{\partial h_\infty}.\frac{\partial h_\infty}{\partial V} + \frac{\partial h}{\partial \tau_h}.\frac{\partial \tau_h}{\partial V}$$

The maximum change in voltage, i.e. the difference between v^* and v, is given by the granularity of voltage values that were used in PEFT. When 20000 uniformly spaced values are taken in $[V_{res}, V_{max}]$, $max(|v - v^*|) \approx 0.007$. For $\mathcal{H}_{Na}$, $\frac{\partial m_\infty}{\partial V} \leq 0.001$, $\frac{\partial tau_m}{\partial V} \leq 0.0015$, $\frac{\partial h_\infty}{\partial V} \approx 0.0001$ and $\frac{\partial tau_h}{\partial V} \leq 0.0014$. For $\mathcal{H}_K$, $\frac{\partial m_\infty}{\partial V} \leq 4.84 \times 10^{-5}$, $\frac{\partial tau_m}{\partial V} \leq 6.73 \times 10^{-5}$, $\frac{\partial h_\infty}{\partial V} \approx 2.79 \times 10^{-9}$ and $\frac{\partial tau_h}{\partial V} \leq 2.3 \times 10^{-6}$.

Performing a similar analysis for bounding the divergence between $\mathcal{M}^v_{Na}$ and $\mathcal{M}^{v^*}_{Na}$ is slightly more complicated. The solutions of the two 13×13 systems depends the matrix exponentials $e^{A(v)}$ and $e^{A(v^*)}$, where A is the rate matrix defined in Definition 2. The matrix exponentials are determined by the spectrum (eigenvalues) of A. Thus the sensitivity of the solutions of

$\mathcal{M}_{Na}^{v}$ and $\mathcal{M}_{Na}^{v^*}$ can be bound by bounding the change in the spectrum of A due to a change in voltage from v to v^*. Bauer-Fike theorem [2] can be used to bound the perturbation in the spectrum. The maximum change in the eigenvalue is bound by a factor of $max(|v - v^*|) \approx 0.007$.

Combining the three components of errors, we get $\delta_{Na} = 6 \times 10^{-3}$. Note that this is a conservative bound and is much more than the the empirical evidence shown in Section 4. A similar analysis can be performed to bound the divergence of $\mathcal{M}_K$ and $\mathcal{H}_K$, to get $\delta_K = 0.15$. □

6. Conclusions and Future Work

We constructed two-state HH-type models, $\mathcal{H}_{Na}$ and $\mathcal{H}_K$, that can replace the corresponding detailed ion channel models, $\mathcal{M}_{Na}$ (13-state) and $\mathcal{M}_K$ (10-state) respectively, within the IMW model. Our ongoing work involves adapting the PEFT procedure to make the abstractions more robust to different types of input stimuli.

The reduction was formalized by proving the abstract and the concrete models to be approximately bisimilar. This notion of system equivalence can be used for compositional reasoning. We are working on computing Lyapunov functions that characterize input-to-state stability of the detailed and abstract models. These functions will then be used to prove that the alternate models can be composed with the rest of the IMW model.

In the future, we plan to use the *towers of abstraction* constructed from the strategy outlined in the paper, for insightful analysis of cardiac models.

References

[1] E. Bartocci, E. Cherry, J. Glimm, R. Grosu, S. A. Smolka, and F. Fenton. Toward real-time simulation of cardiac dynamics. In *Proceedings of the 9th International Conference on Computational Methods in Systems Biology, CMSB'2011*, pages 103–112. ACM, 2011.

[2] F. L. Bauer and C. T. Fike. *Norms and Exclusion Theorems*. Numerische Matematik, 1960.

[3] A. Bueno-Orovio, E. M. Cherry, and F. H. Fenton. Minimal model for human ventricular action potentials in tissue. *Journal of Theoretical Biology*, 253(3):544–560, 2008.

[4] E. M. Cherry and F. H. Fenton. Visualization of spiral and scroll waves in simulated and experimental cardiac tissue. *New Journal of Physics*, 10:125016, 2008.

[5] F. H. Fenton and E. M. Cherry. Models of cardiac cell. *Scholarpedia*, 3:1868, 2008.

[6] J. Fisher, N. Piterman, and M. Y. Vardi. The only way is up. In *Proceedings of the 17th International Conference on Formal methods*, FM'11, pages 3–11, Berlin, Heidelberg, 2011. Springer-Verlag.

[7] A. Girard. Controller synthesis for safety and reachability via approximate bisimulation. *Automatica*, 48:947–953, 2012.

[8] A. Girard and G. J. Pappas. Approximate bisimulations for nonlinear dynamical systems. In *Proceedings of CDC'05, the 44th International Conference on Decision and Control*, Seville, Spain, December 2005. IEEE.

[9] A. Girard and G. J. Pappas. Approximate bisimulation relations for constrained linear systems. *Automatica*, 43:1307–1317, 2007.

[10] A. Girard and G. J. Pappas. Approximation metrics for discrete and continuous systems. *IEEE Transactions on Automatic Control*, 52(5):782 –798, May 2007.

[11] J. L. Greenstein, R. Wu, S. Po, G. F. Tomaselli, and R. L. Winslow. Role of the calcium-independent transient outward current I_{to1} in shaping action potential morphology and duration. *Circulation Research*, 87(11):1026–1033, Nov. 2000.

[12] R. Grosu, G. Batt, F. Fenton, J. Glimm, C. L. Guernic, S. A. Smolka, and E. Bartocci. From cardiac cells to genetic regulatory networks. In *Proc. of CAV'11, the 23rd International Conference on Computer Aided Verification*, LNCS, Cliff Lodge, Snowbird, Utah, USA, July 2011. Springer.

[13] A. L. Hodgkin and A. F. Huxley. A quantitative description of membrane current and its application to conduction and excitation in nerve. *Journal of Physiology*, 117:500–544, 1952.

[14] L. A. Irvine, M. S. Jafri, and R. L. Winslow. Cardiac sodium channel markov model with tempretature dependence and recovery from inactivation. *Biophysical Journal*, 76:1868–1885, 1999.

[15] V. Iyer, R. Mazhari, and R. L. Winslow. A computational model of the human left-ventricular epicardial myocytes. *Biophysical Journal*, 87(3):1507–1525, 2004.

[16] Jasmin Fisher, David Harel, and Thomas A. Henzinger. Biology as reactivity. *Communications of the ACM*, 54(10):72–82, October 2011.

[17] J. Keener. Invariant manifold reductions for markovian ion channel dynamics. *Journal of Mathematical Biology*, 58(3):447–457, July 2009.

[18] C.-C. Kuo and B. P. Bean. Na^+ channels must deactivate to recover from inactivation. *Neuron*, 12:819–829, 1994.

[19] C. H. Luo and Y. Rudy. A dynamic model of the cardiac ventricular action potential. I. Simulations of ionic currents and concentration changes. *Circulation Research*, 74(6):1071–1096, June 1994.

[20] MATLAB ODE45 solver. *Version 7.10.0 (R2010a)*. The MathWorks Inc., Natick, Massachusetts, 2010.

[21] MATLAB Open curve fitting toolbox (cftool). *Version 7.10.0 (R2010a)*. The MathWorks Inc., Natick, Massachusetts, 2010.

[22] C. J. Myers. *Engineering Genetic Circuits*. CRC Press, 2010.

[23] National Science Foundation (NSF). Computational Modeling and Analysis of Complex Systems (CMACS). http://cmacs.cmu.edu.

[24] K. H. W. J. ten Tusscher, D. Noble, P. J. Noble, and A. V. Panfilov. A model for human ventricular tissue. *American Journal of Physiology*, 286:H1573–H1589, 2004.

[25] J. van den Hof. *System theory and system identification of compartmental systems*. PhD thesis, University of Groningen, Netherlands, November 1996.

Appendix A. Stability properties of voltage-controlled CTMCs for Ion Channels

In this section, we use compartmental systems theory [25] to state and prove stability properties of the constant-voltage ion channel models $\mathcal{M}_{Na}^{v}$ and $\mathcal{M}_{K}^{v}$. This in turn justifies the simulation strategy used in PEFT, i.e. finite-length simulations of $\mathcal{M}_{Na}^{v}$ and $\mathcal{M}_{K}^{v}$ are sufficient to obtain the approximately bisimilar HH-type abstractions $\mathcal{H}_{Na}^{v}$ and $\mathcal{H}_{K}^{v}$.

Theorem 3. *Let $A_x(v)$, be the rate matrix of the corresponding dynamical system M_x, $x \in \{Na, K\}$, as per Definitions 2 and 3. For all the values of the bounded input $v \in [V_{res}, V_{max}]$, $A_x(v)$ has exactly one eigenvalue that is 0 and the real part of all the other eigenvalues is negative.*

Proof. First, we will prove a lemma showing that the rate matrices $A_x(v)$ are *compartmental matrices* for $v \in [V_{min}, V_{max}]$.

Lemma 4. *The rate matrix $A_x(v)$ is a compartmental matrix for $v \in [V_{min}, V_{max}]$.*

Proof. A square matrix $M \in \mathbb{R}^{n \times n}$ is called a compartmental system if it satisfies the following properties:

1. All the non-diagonal entries are greater than or equal to 0, i.e $M_{ij} \geq 0$ for $i = 1, \ldots, n, j = 1, \ldots, n, i \neq j$.

2. Sum of the entries along all the columns is less than or equal to 0, i.e. $\sum_{i=1}^{n} M_{ij} \leq 0$, $j = 1, \ldots, n$.

The M_{ij} entry of the matrix is interpreted as the rate of flow of mass from the j^{th} compartment to the j^{th} compartment, $i \neq j$. The diagonal entry M_{ii} is the total rate of outflow from the i^{th} compartment.

For the rate matrices $A_x(v)$, the first property is satisfied as the non-diagonal entries on the i^{th} row of $A_x(v)$ represent incoming transfer rates for state i. These rates are positive as they are exponential functions of the input v. For $\mathcal{M}_{Na}$ and $\mathcal{M}_{K}$, these functions are listed in Tables 1 and 2 respectively.

Consider the j^{th} column of $A_x(V)$. The entry $A_{x,ij}$, $i \neq j$ denotes the transfer rate from state j to state i. The diagonal entry of this column $A_{x,jj}$ is the negated sum of all the outgoing rates from state j. Thus, the sum of every column is 0. □

Lemma 5. *The rate matrix $A_x(v)$ is irreducible for $v \in [V_{min}, V_{max}]$.*
Proof. Irreducibility of $A_x(v)$ can be proved using a graph-theoretic argument. We construct a directed graph $G_x^v(W, E)$, where the set of vertices W corresponds to the states of M_x. The set of edges E is constructed as follows. An edge, e_{ij}, from vertex i to vertex j, $i, j = 1, \ldots, n$ exists if $A_{x,ij}(v) \neq 0$.

From linear algebra, we know that the matrix $A_x(v)$ is irreducible if and only if $G_x^v(V, E)$ is connected, i.e. there is a path between every pair of vertices.

If there is an edge from state i to state j of M_x, then the transfer rate $A_{x,ij}(v)$ does not become 0 for any value of v as it an exponential function of v. Also, for a given value of $v \in [V_{min}, V_{max}]$, the corresponding graph G_x^v always remains connected. Thus $A_x(v)$ is irreducible for all $v \in [V_{min}, V_{max}]$. □

Now we introduce the concept of a *trap* of a compartmental system. A trap is a compartment or a set of compartments from which there are no transfers or flows to the environment nor to the compartments that are not in that set. A formal definition is as follows. Let S be a linear compartmental system consisting of compartments $C_1, C_2, \ldots, C_n$. Let $T \subseteq S$, be a subset of the compartments. We number the compartments such that T consists of the compartments $C_m, C_{m+1}, \ldots, C_n$ for $m \leq n$. Let $F \in \mathbb{R}^{n \times n}$ be the rate matrix consistent with the new numbering. The subset T is a trap if and only if $F_{ij} = 0$ for (i, j) such that $j = m, m+1, \ldots, n$ and $i = 0, 1, \ldots, m-1$. A trap is said to be *simple* is it does not strictly contain any traps.

Lemma 6. *The only trap in $A_x(v)$ is the set of all states.*

Proof. As $A_x(v)$ is irreducible, as per Lemma 5, flow between any pair of compartments is nonzero. Thus the only trap is the set of all compartments, □

The proof of the Theorem 3 now follows from Theorems 2.2.4 and 2.2.6 of [25]. Prerequisite conditions have been proved in Lemmas 5 and 6. □

A corollary of Theorem 3 is that for all values of the input $V \in [V_{min}, V_{max}]$ the constant voltage autonomous dynamical systems $\mathcal{M}_{Na}$ and $\mathcal{M}_K$ have stable equilibria. A 0 eigenvalue does not make $A_{Na}(v)$ and $A_K(v)$ Hurwitz, and thus does not lead to asymptotic stability of the equilibria.

Appendix B. List of Abbreviations

DEM Differential Equation Model

IMW Iyer, Mazhari and Winslow

MM Minimal Model

AP Action Potential

HH Hodgkin-Huxley

VCE Voltage Clamp Experiment

CTMC Continuous Time Markov Chain

PEFT Parameter Estimation from Finite Traces

RFI Rate Function Identification

Appendix C.

Nomenclature

$\alpha_h(V)$ The rate of opening of an inactivating (h-type) subunit in an HH-type model.

$\alpha_m(V)$ The rate of opening of an activating (m-type) subunit in an HH-type model.

$\beta_h(V)$ The rate of closing of an inactivating (h-type) subunit in an HH-type model.

$\beta_m(V)$ The rate of closing of an activating (m-type) subunit in an HH-type model.

λ The degree of activation in an HH-type model, 3 for $\mathcal{H}_{Na}$ and 4 for $\mathcal{H}_K$.

$\mathcal{H}$ The HH model for Squid neurons.

$\mathcal{H}_K$ The 2-state HH-type abstraction identified for $\mathcal{M}_K$ using PEFT and RFI.

$\mathcal{H}_K^v$ The constant-voltage version of $\mathcal{H}_K$, where $V = v$.

$\mathcal{H}_{Na}$ The 2-state HH-type abstraction identified for $\mathcal{M}_{Na}$ using PEFT and RFI.

$\mathcal{H}_{Na}^v$ The constant-voltage version of $\mathcal{H}_{Na}$, where $V = v$.

$\mathcal{M}_K$ The 10-state voltage-controlled CTMC for the sodium current $I_{Kv4.3}$.

$\mathcal{M}_K^v$ The constant-voltage version of $\mathcal{M}_K$, where $V = v$.

$\mathcal{M}_{Na}$ The 13-state voltage-controlled CTMC for the sodium current I_{Na}.

$\mathcal{M}_{Na}^v$ The constant-voltage version of $\mathcal{M}_{Na}$, where $V = v$.

$\overline{g}_{Na}$ Maximum conductance of the sodium channel.

h Variable used in HH-type models for measuring the extent of inactivation.

$I_{Kv4.3}$ The potassium current, component of the I_{to1} current, and modeled using the voltage-controlled CTMC $\mathcal{M}_K$ in the IMW model.

I_{Na} Sodium current, modeled using the voltage-controlled CTMC $\mathcal{M}_{Na}$ in the IMW model.

m Variable used in HH-type models for measuring the extent of activation.

O_H Conductance of the HH-type channel, given by $\{m(V,t)\}^\lambda h(V,t)$.

O_K The conductance (observable output) of $\mathcal{M}_K$, given by $O_K = O$, the occupancy probability of the state labeled O.

O_{Na} The conductance (observable output) of $\mathcal{M}_{Na}$, given by $O_{Na} = O_1 + O_2$, the occupancy probabilities of the states labeled O_1 and O_2.

V Transmembrane potential of a cardiac myocyte.

V_{max} The maximum potential reached by cardiac myocytes during an AP.

V_{Na} Nernst potential for sodium.

V_{res} The resting potential for cardiac myocytes.

A_K The 10×10 rate matrix for $\mathcal{M}_K$.

A_{Na} The 13×13 rate matrix for $\mathcal{M}_{Na}$.

***Revision Note**

Summary of changes made in the revised version

1. The Background section, which introduces the ionic channel models, has been simplified. The right-inlay of Figure 2 no longer shows the comparison of the sodium current and other currents during the upstroke phase. Also, the notation has been simplified for better readability.

2. The Results section now includes a table summarizing the empirical evidence of the substitutivity of the detailed and abstract ion channel components within the whole-cell IMW model.

3. In Section 5, the section on approximate bisimulation, we no longer represent the ion channel models as labeled transition systems, as done in the previous version. Approximate bisimulation (Definition 4) is defined directly on dynamical systems. Consequently, the notation has been considerably simplified.

4. The proof of approximate bisimulation does not use discrete-time arguments, as done previously. We consider the time interval $[t, t + \delta t]$ and prove bisimilarity as $\delta t \to 0$.

5. The lemmas and theorems pertaining to the stability properties of the detailed ion channel models have been moved from Section 5 to Appendix A.

6. Our abstraction technique, consisting of a two-level fitting process, can be adapted to handle the case where arbitrary functions map states of the detailed ion channel models to their outputs. A detailed discussion of this point has been added to the end of Section 3, the methodology section.

7. We have included a list of abbreviations in Appendix B.

8. A list of model variables and parameters can be found in Appendix C.

9. We now specify the domain of the variables as part of the model definition.

10. The abbreviations in the Introduction that were not subsequently used have been removed.

11. Sections 2 (Background), 3 (the parameter-fitting process), 4 (Results) and 5 (approximate bisimulation) have been completely rewritten.